Supporting Information

Vakarelski et al. 10.1073/pnas.1005937107

SI Text

SI Methods. ***Atomic force microscopy force measurements.*** The bubble colloidal probe technique developed earlier (1) for the Asylum MPF-3D Atomic Force Microscope (AFM) was used in the present dynamic coalescence experiments.

Substrates were circular glass slides (35 mm liquid cell substrates, Asylum Research) mildly hydrophobized by immersing them briefly in a 3 mM solution of octadecyltrichlorosilane in heptane to give water contact angles in the range of 20–60° after treatment. The degree of hydrophobicity of the slides could be adjusted by further brief exposure to a UV light source in a closed chamber. The rectangular silicon cantilevers were custom-made with a circular end platform (Fig. 1*B*) to facilitate easy bubble pickup and precise, secure anchoring. The cantilever dimensions were $450 \times 50 \times 2$ μm and the circular platform had a diameter of 65 μm with a 20-nm-thick gold coating. The gold-coated platform was hydrophobized by immersing the cantilevers for several hours in 10 mM n-decanethiol solution in ethanol. The cantilever spring constant was measured using the Hutter and Bechhoefer (2) thermal tune function of the Asylum MFP-3D software.

Electrolyte solutions were prepared using Millipore water of specific resistance greater than 18.2 MΩ cm and sodium nitrate (NaNO3 $NaNO_3$ 99 + %, Aldrich) baked at 250 °C for 5 h to remove possible organic contaminations.

The hydrophobized slide samples were placed in a Pyrex glass Petri dish and covered with about 5 mm of the electrolyte solution. Bubbles on the glass surface were generated by ultrasonication with an ELAC Nautic ultrasonic device with radio frequency generator type LVG 60-10. A 347 kHz frequency signal of approximately 9 W output power applied for 10–30 s resulted in multiple bubbles covering the glass substrate surface (1).

Immediately after bubble generation, the Petri dish was moved onto the Asylum AFM sample stage. A chosen bubble was picked from the surface and anchored on the hydrophobized circular platform of the cantilever to form a bubble colloidal probe (Fig. 1*A*). Before each bubble collision measurement, microscopy photographs of the cantilever and substrate bubble were taken using the inverted microscope optical system attached to the AFM (Fig. S1 and Fig. 1 *C* and *D*), from which the radius of the cantilever bubble, R_c, and the surface bubble, R_s, as well as bubble-substrate contact zone radius, a, can be measured. The contact angles θ_c, θ_s (Fig. 1*D*) deduced from these measurements are in the range of 130–160°.

The bubble collision force measurements were carried out in the same manner as previously described for force measurements between emulsion drops or bubbles (3, 4). After careful alignment between the bubbles on the cantilever and on the surface, the cantilever bubble was driven toward the surface bubble from a large initial separation by controlled changes in the cantilever-substrate separation, $X(t)$, at a scan rate of up to 50 μm/s. Time variations of cantilever deflections, converted to forces via the measured spring constant, were recorded for a single approach/retract cycle. Bubble proximity was indicated by the appearance of a hydrodynamic force maximum at the change of scan direction from the approach to the retraction phase, followed by an attractive hydrodynamic minimum before the bubbles separate at the conclusion of the retraction phase (Fig. 2*A*, the noncoalescing case, curve JKLM, where for clarity only 10% of the recorded data points have been plotted). In subsequent scans with the same bubble pair, bubble coalescence can be made to occur in one of three modes:

1. maintaining a constant scan size of around 2 μm and gradually decreasing the initial separation, h_o, until coalescence would occur during retraction (Fig. 2*A* coalescing case, curve EFGH);
2. increasing the scan size to around 6 μm, which would cause coalescence to occur before the start of the retraction phase (Fig. 2*B*, right axis, curve PQRS); or
3. using the Asylum force measurement "dwell mode," in which the cantilever motion was stopped at a set point of the approach scan and coalescence would occur in this approach-stop mode (Fig. 2*B*, left axis, curve WXYZ).

The Asylum MFP-3D AFM is equipped with a linear variable differential transformer (LVDT) which reports the actual location, $X(t)$, of the piezo-electric actuator as it moves through the approach/retract cycle of a force-displacement measurement with $t = 0$ being the start of the approach/retract cycle. As the LVDT piezo-electric actuator position, $X(t)$, does not vary linearly with the time (5), a more fundamental way to present and analyze our experiments is to consider the time variation of the force as measured by the cantilever deflection (Fig. 2 *A* and *B*) (5).

Theoretical model. The model for dynamic interactions between the bubbles had been developed earlier (6, 7). Hydrodynamic interaction between the bubbles was modeled with the Reynolds lubrication theory for the movement of water with dynamic viscosity, μ, in the thin film between the bubbles. With the no-slip boundary condition at the bubble surface and assuming axial symmetry is maintained during head-on bubble–bubble collisions, the film thickness, $h(r,t)$, and the hydrodynamic pressure, $p(r,t)$, were related by

$$\frac{\partial h}{\partial t} = \frac{1}{12\mu}\frac{\partial}{\partial r}\left(rh^3\frac{\partial p}{\partial r}\right).$$

The Young–Laplace equation

$$\frac{\sigma}{2r}\frac{\partial}{\partial r}\left(r\frac{\partial h}{\partial r}\right) = \frac{2\sigma}{R} - p - \Pi,$$

where $R^{-1} = (R_c^{-1} + R_s^{-1})/2$ was used to describe deformations of the bubbles (with constant interfacial tension, σ) due to the hydrodynamic pressure, $p(r,t)$, and the disjoining pressure, $\Pi[h(r,t)]$, that accounted for the surface force per unit area between the bubbles. The contribution from van der Waals–Lifshitz interaction to the vapor–water–vapor disjoining pressure between the bubble surfaces was calculated using the complete Lifshitz formula with full account of electromagnetic retardation effects (8) and screening by electrolyte for the zero frequency term (9):

$$\Pi_{vdW}(h) = \Pi_{vdW0}(h) - \frac{kT}{\pi c^3}\sum_{n=1}^{\infty}\varepsilon^{3/2}\xi_n^3\int_1^{\infty}p^2\{[De^x - 1]^{-1} + [\tilde{D}e^x - 1]^{-1}\}dp,$$

where

$$D = \left(\frac{s + p/\varepsilon}{s - p/\varepsilon}\right)^2 \qquad \tilde{D} = \left(\frac{s+p}{s-p}\right)^2 \qquad s = \sqrt{p^2 - 1 + \varepsilon^{-1}}$$

$$x = 2p\xi_n\varepsilon^{1/2}h/c$$

and the zero frequency term is

$$\Pi_{vdW0}(h) = -\frac{kT}{2\pi}\int_0^\infty \frac{sZe^{-2qh}}{1-Ze^{-2qh}}pdp,$$

where

$$Z = \left(\frac{p-q\varepsilon(0)}{p+q\varepsilon(0)}\right)^2 \qquad q = \sqrt{p^2+\kappa^2}.$$

The relative permittivity of water $\varepsilon = \varepsilon(i\xi_n)$ is to be evaluated at imaginary frequencies $i\xi_n = i(2\pi nkT/\hbar)$ where k is Boltzmann's constant, $(2\pi\hbar)$ is Planck's constant, c is the velocity of light in vacuum, T is the absolute temperature, and $(1/\kappa)$ is the usual Debye screening length that depends on electrolyte concentration. The quantity $\varepsilon(i\xi_n)$ for water has been constructed from recent dielectric data (10). At small separations (<1 nm), the disjoining pressure has the nonretarded form $\Pi_{vdW}(h) \cong -A/(6\pi h^3)$, where the Hamaker constant, $A = 5.63\times10^{-20}$ J, or $A = 5.01\times10^{-20}$ J if the zero frequency term was omitted (10). At 0.5 M, the zero frequency term is negligibly small.

The piezo-electric actuator displacement $X(t)$ enters via the boundary condition imposed outside the interaction zone of the water film at $r = r_{\max}$ between the interacting bubbles

$$\frac{dX}{dt} = \frac{\partial h}{\partial t} + \frac{\alpha}{2\pi\sigma}\frac{dF}{dt},$$

where (7)

$$\alpha = 2\log\left(\frac{r_{\max}}{2\sqrt{R_cR_s}}\right) + B(\theta_c) + B(\theta_s)$$

$$B(\theta) = 1 + \frac{1}{2}\log\left(\frac{1+\cos\theta}{1-\cos\theta}\right).$$

This boundary condition follows from a constant volume constraint on the bubbles. The governing equations can be solved numerically by the method of lines in the domain $0 < r < r_{\max}$ (6). The value of $r_{\max}$ is chosen to be larger than the interaction zone between the bubbles where asymptotic forms of the pressure are known, but otherwise, the solution does not depend on its precise value. Implicit in this model is the assumption that all deformations and separations are small compared to the radii of the bubbles, a condition well satisfied in the present experiments.

Sensitivity to the initial separation. The design of the AFM allows the value of the initial separation, h_o, between the bubbles to be set coarsely within a desired range but not to high precision. We determine the value of h_o by ensuring that the model can reproduce in all key features of the force curve, namely, the magnitude and location of the repulsive force maximum on approach, the depth and location of the attractive force minimum, or the location and force magnitude at the point of coalescence on retraction. In Fig S2, we show variations of the predicted force curves for the two experiments in Fig 2*A* due to changing the optimal initial values of $h_o = 2.45$ or 2.05 μm by ±0.1 μm. By fitting to the entire force curve, we can determine the value of h_o to within ±0.01 μm.

Collision results for $NaNO_3$ at 0.02 M. At a low concentration, e.g., 0.02 M, bubble collisions in $NaNO_3$ are all stable and do not coalesce. According to our theoretical model, a surface potential of −25 mV would provide sufficient electrical double-layer repulsion to prevent stability. Sample results and corresponding predictions of our model are shown in Fig S3. The observed behavior is consistent with intuitions provide by the Deryaguin–Landau–Verwey–Overbeek theory of colloid stability.

Coalescence results for $NaNO_3$ and $NaClO_4$ at 0.5 M. Bubble stability studies of bubble swarms show that $NaNO_3$ inhibited bubble coalescence at concentrations above 0.1 M whereas $NaClO_4$ has no effects on bubble at any concentration (11). In Fig. S4, we show coalescence on separation results in these two salts at 0.5 M with essentially identical coalescence behavior in both cases. The theoretical predictions fitted the force curve well. The magnitudes of the disagreement between predicted and experimental coalescence time are typical of that show in Fig. 3 in the main text.

Animated visualization of results. To help the reader visualize the bubble collisions, animations of how the surfaces of the bubble evolve during the collision and coalescence of two bubbles for the three different coalescence cases, the force curve (EFGH) in Fig 2*A* and both force curves in Fig. 2*B* of the main text are available as movie files. These animations are based on calculations using the theoretical model developed in this work and span the time frame of the collision until the point of coalescence. A schematic of the force versus time for these collisions are also included in the animation. As the profiles of the bubbles deform in compression, the color of the lines lighten and as they deform in tension the color of the lines darken.

These animations demonstrate how the bubbles flatten in compression and form a relatively flat thin film as they approach due to repulsive hydrodynamic drainage forces. As the bubbles retract in curve EFGH of Fig 2*A*, the reversal of the hydrodynamic drainage force causes the bubbles to continue to reduce the separation between the bubbles and forms a gradual dimple on both bubble interfaces. The films suction continues to drive the barrier rims closer together until the separation between the rims of the dimples becomes sufficiently close for the van der Waals–Lifshitz attractive forces to induce coalescence of the bubbles at the rims of the dimples.

1. Vakarelski IU, et al. (2008) Bubble colloidal AFM probes formed from ultrasonically generated bubbles. *Langmuir* 24:603–605.
2. Hutter JL, Bechhoefer J (1993) Calibration of atomic-force microscope tips. *Rev Sci Instrum* 64:1868–1873.
3. Dagastine RR, et al. (2006) Dynamic forces between two deformable oil droplets in water. *Science* 313:210–213.
4. Manor O, et al. (2008) Dynamic forces between bubbles and surfaces and hydrodynamic boundary conditions. *Langmuir* 24:11533–11543.
5. Webber GB, et al. (2008) Measurements of dynamic forces between drops with the AFM: Novel considerations in comparisons between experiment and theory. *Soft Matter* 4:1270–1278.
6. Manica R, et al. (2008) Transient responses of a wetting film to mechanical and electrical perturbations. *Langmuir* 24:1381–1390.
7. Manica R, et al. (2008) Hydrodynamic forces involving deformable interfaces at nanometer separations. *Phys Fluids* 20:032101-1–032101-12.
8. Dzyaloshinskii IE, Lifshitz EM, Pitaevskii LP (1961) The general theory of van der Waals forces. *Adv Phys* 10:165–209.
9. Mitchell DJ, Richmond P (1974) A general formalism for the calculation of free energies of inhomogeneous dielectric and electrolytic systems. *J Colloid Interface Sci* 46:118–127.
10. Dagastine RR, Prieve DC, White LR (2000) The dielectric function for water and its application to van der Waals forces. *J Colloid Interface Sci* 231:351–358.
11. Craig VSJ (2004) Bubble coalescence and specific-ion effects. *Curr Opin Colloid In* 9:178–184.

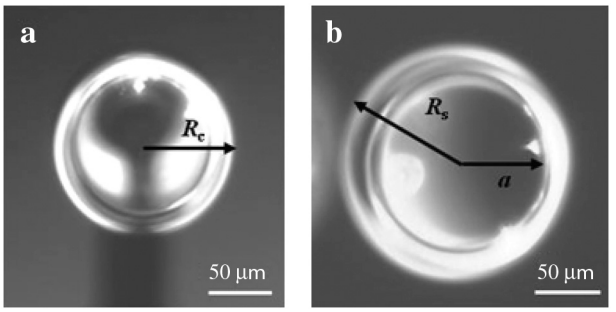

Fig. S1. Typical microscopic images used to determine the bubbles size and contact angles. (*A*) Cantilever attached bubble. (*B*) Surface anchored bubble. Images are taken through the glass substrate using the Asylum inverted microscope.

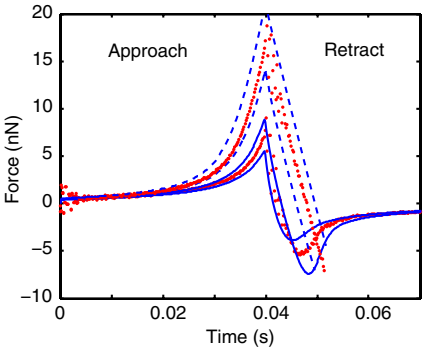

Fig. S2. Sensitivity of the theoretical force curves to variations of the initial separation, h_o, by ±0.1 μm in modeling the results in Fig 2*A*.

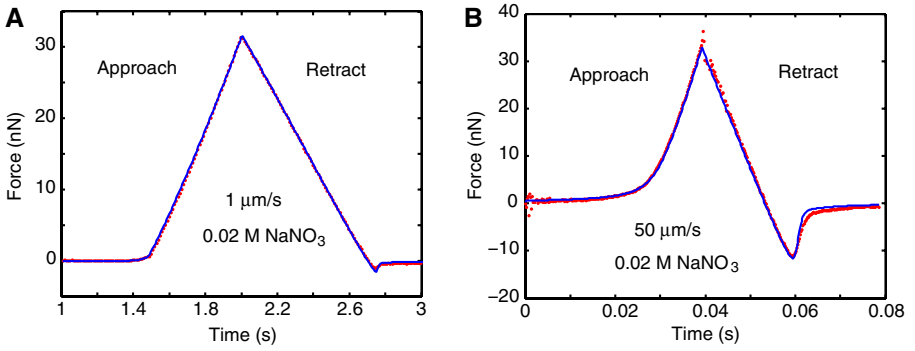

Fig. S3. A comparison of experimental (• • •) and predicted (——) forces between the two bubbles (radii 54, 72 μm; contact angles 155 and 141°) during stable collisions in an approach-retract cycle in 0.02 M $NaNO_3$ at two different nominal velocities: (*A*) 1 μm/s, $h_o = 1.72$ μm; (*B*) 50 μm/s, $h_o = 1.62$ μm. The maximum piezo-electric actuator displacement is 2.5 μm in both cases.

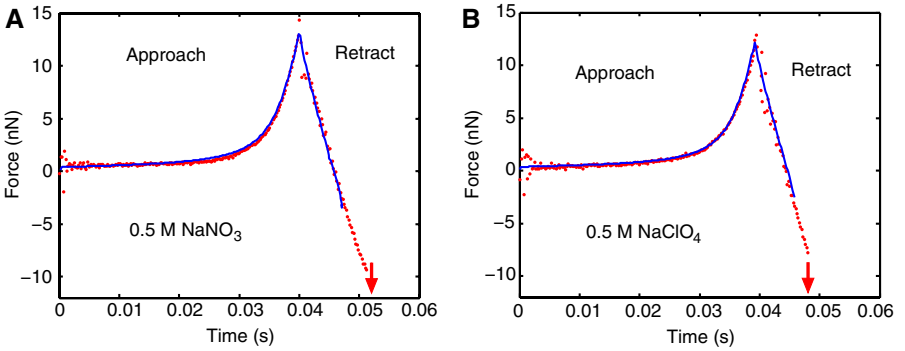

Fig. S4. A comparison of experimental (• • •) and predicted (——) forces between the two bubbles that coalesced on separation in during an approach-retract cycle at the same nominal velocity of 50 μm/s in (*A*) 0.5 M $NaNO_3$ with bubble radii 44 and 86 μm, contact angles 148 and 146°, initial separation $h_o = 2.06$ μm; (*B*) 0.5 M $NaClO_4$ with bubble radii 48 and 64 μm, contact angles 150 and 148°, initial separation $h_o = 2.12$ μm. The maximum piezo-electric actuator motor displacement is 2.5 μm in both cases. The time of coalescence is indicated by the downward arrow.

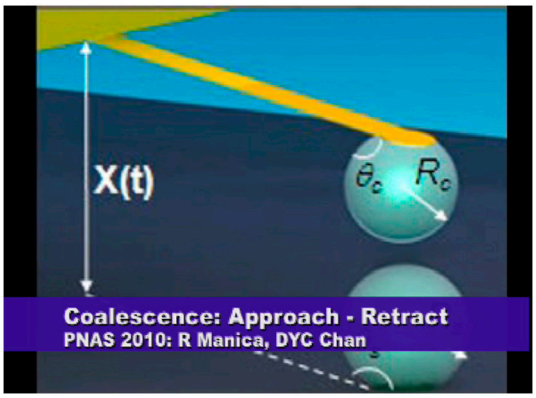

Movie S1. Animation of calculated bubble surface evolution prior to the coalescence of two bubbles for the approach-retract collision corresponding to curve EFGH in Fig. 2*A*. For reference, the corresponding force versus time for this collision is also included in the animation.
Movie S1 (MP4)

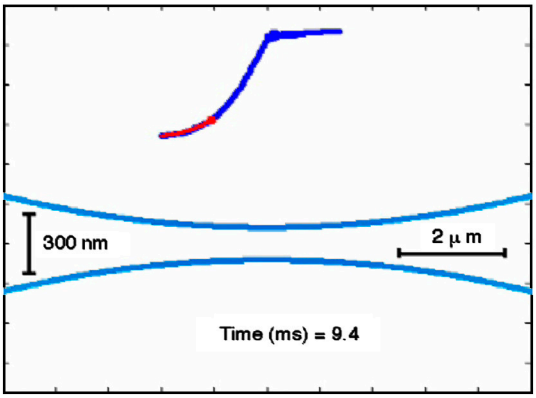

Movie S2. Animation of calculated bubble surface evolution prior to the coalescence of two bubbles for the approach-stop collision corresponding to curve WXYZ in Fig. 2*B*, left-hand axis. For reference, the corresponding force versus time for this collision is also included in the animation.
Movie S2 (MP4)

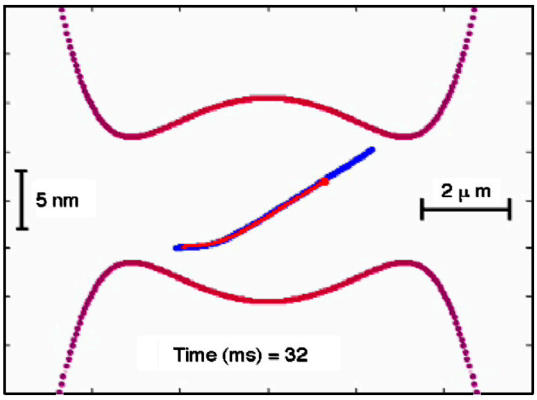

Movie S3. Animation of calculated bubble surface evolution prior to the coalescence of two bubbles for the approach only collision corresponding to curve PQRS in Fig. 2*B*, right-hand axis. For reference, the corresponding force versus time for this collision is also included in the animation.
Movie S3 (MP4)